SIMULATION AND ANALYSIS OF THE THERMAL AND DEFORMATION BEHAVIOUR OF "AS-RECEIVED" AND "HYDRIDED" PRESSURE TUBES USED IN THE CIRCUMFERENTIAL TEMPERATURE DISTRIBUTION EXPERIMENTS (END OF LIFE/PRESSURE TUBE BEHAVIOUR)

W.C. MUIR and M.H. BAYOUMI

Ontario Hydro, Reactor Safety and Operational Analysis Department
700 University Avenue, Toronto, Ontario, M5G 1X6

ABSTRACT

It is postulated that in-reactor pressure tubes may be subjected to radiation damage and dissolved deuterium which could change the pressure tube characteristics and lead to different behaviour than that of as-received pressure tubes under large LOCA conditions. A hydrided pressure tube was used to study the effect of dissolved hydrogen on thermal-mechanical behaviour. In the experiment, simulating an in-reactor (hydrided) pressure tube with circumferential differential temperature under boil-off conditions, the pressure tube ballooned into contact with the calandria tube. The pressure tube used in this experiment was hydrided in a furnace to a nominal value of 200 μg/g dissolved hydrogen. This test was a repeat of the first supplementary boil-off test (S-5-1) [1] which used an as-received pressure tube. The objective of this paper is to analyze the results obtained from the simulation of this Boil-Off test using the SMARTT [2] computer code and to examine the effect of hydriding on the thermal and ballooning behaviour of the pressure tube by comparison with the results obtained from test S-5-1. A discussion of the results obtained from this comparison is presented together with an analysis of their application to the analysis of pressure tube behaviour in CANDU reactors.

INTRODUCTION

In a number of postulated loss-of-coolant accident (LOCA) scenarios, some fuel channels are predicted to initially experience periods of stratified flow. During this period, the steam generated will flow to the top portion of the pressure tube and thereby expose this region of the pressure tube to superheated steam. The exposed part of the pressure tube and fuel elements will heat up rapidly due to fuel decay power where the main heat removal mechanisms are by radiation and steam convection. As the liquid level drops further, the pressure tube continues to become hotter at the top while the lower part below the liquid level remains at or below saturation temperature. Subsequently, the channel experiences a period of sustained liquid boil-off after the feeders are drained. In this period, the remaining liquid in the channel and end-fittings continues to boil away and the extent of fuel element over-heating progressively increases. Steam venting may occur through one or both feeders. During this period, a circumferential temperature gradient develops around the pressure tube which could result in a nonuniform or localized pressure tube strain that could lead to failure of the pressure tube before ballooning into contact with the calandria tube.

Three distinct phases of feeder draining have been identified [3], namely, steady steaming, steam cooling and boil-off. In the steady-steaming phase that corresponds to the early stages of feeder drainage, the inlet feeder and the inlet end-fittings are filled with liquid that is close to saturation. The outlet header is completely voided with no liquid to counter flow down the outlet feeder and, consequently, reducing the established density driving head. In the steam cooling phase, the liquid level drops below the inlet feeder connection to the inlet header and is characterized by a steadily decreasing density driving head as the liquid level in the feeder decreases. In this phase, depending on the inlet header conditions, a decreasing flow rate of single or two-phase flow from the inlet header into the channel is established. In the boil-off stage, the channel and end-fittings experience a period of sustained boil off in which the extent of overheating of the fuel element progressively increases.

The pressure tube circumferential temperature gradient experimental program (PT-DELTA T) has been ongoing at AECL-WNRE under COG (CANDU Owners Group) to investigate the potential of pressure tube rupture during

ballooning. The experimental results were used to validate the computer code SMARTT (Simulation Method for Azimuthal and Radial Temperature Transients) [2] which is one of the analytical tools used in the safety and licensing analysis of CANDU reactors to show that a postulated loss-of-coolant accident does not lead to rupture of the fuel channels.

Five experimental series have been completed at AECL-WNRE under COG to address all of the various phases of feeder draining. The Boil-off Series was designed to examine fuel channel response when the coolant flow is stagnated and the liquid remaining in the channel boils away [4,5] (channel boil-off phase). In the Make-Up Water series, the coolant level is maintained constant by injecting make-up water to balance the steam flow out of the channel to simulate the steady steaming phase (Make-UP Water Series) [6,7]. In the third series, Steam Cooling Series, superheated steam and make-up water are injected simultaneously into one end of the pressure tube. This simulates a postulated LOCA condition in which the inlet header is partially voided, resulting in water and steam flow through the heated fuel channel. In the fourth test series, Variable Make-Up Water Series [8], water is injected into the pressure tube at a controlled and declining rate to study the effect of a gradual decrease in make-up water flow rate and to simulate the decreasing density driving head as the liquid level in the feeder decreases. The third and fourth series of the experiments are designed to simulate different stages of feeder drainage following a large LOCA scenario. The fifth series, the Supplementary Boil-off Series [1,9], was designed to further investigate the thermal-mechanical behaviour of pressure tubes under boil-off conditions after the failure of the pressure tube in the third test of the first series.

The experiments in the first four series employed a 37-element bundle with a concentric-sheath type fuel-element simulator (FES) which was susceptible to electrical failure. Electrical failure of the FESs usually leads to premature pressure tube failure. The fifth experimental series, the Supplementary Boil-off Series [1,9], used more robust graphite-alumina type FESs in a 28-element bundle geometry.

In all of the five experimental series, as-received pressure tubes were used. It is postulated that in-reactor pressure tubes may be subjected to radiation damage and dissolved deuterium which could change the pressure tube characteristics and lead to different behaviour than that of as-received pressure tubes under large LOCA conditions. Since the use of an irradiated pressure tube in the experimental apparatus was not possible, a hydrided pressure tube was used to study the effect of dissolved hydrogen on thermal-mechanical behaviour of the pressure tube. The pressure tube used in the experiment was hydrided in a furnace to a nominal value of 200 μg/g dissolved hydrogen.

In the experiment simulating an in-reactor (hydrided) pressure tube with circumferential differential temperature under boil-off conditions, the pressure tube ballooned into contact with the calandria tube. This test was a repeat of the first supplementary boil-off test (S-5-1) [1] which used an as-received pressure tube. The objective of this paper is to analyze the results obtained from the simulation of this Boil-Off test using the SMARTT [2] computer code and to examine the effect of hydriding on the thermal and ballooning behaviour of the pressure tube by comparison with the results obtained from test S-5-1. Improvements to the SMARTT code are presented. A discussion of the results obtained from this comparison is also presented together with an analysis of their application to the analysis of pressure tube behaviour in CANDU reactors.

OVERVIEW OF THE SMARTT CODE

The SMARTT (Simulation Method for Azimuthal and Radial Temperature Transients) computer code [2] is one of the analytical tools used in the analysis of fuel channel integrity and in the safety analysis of CANDU reactors. The code was developed to predict fuel sheath and pressure tube thermal and mechanical behaviour under asymmetric coolant conditions such as stratified or decreasing coolant flow in the channel. Under such condition, the top portion of the pressure tube and fuel elements are exposed to superheated steam while the bottom portion is cooled with saturated or even slightly subcooled water. Such conditions can lead to non-uniform pressure tube heatup in the circumferential direction. If a highly localized hot spot develops on the pressure tube circumference while the pressure tube is under going transverse strain (ballooning), the pressure tube could rupture prior to contacting the calandria tube. The code predicts the pressure tube circumferential temperature distribution and its effect on pressure

tube ballooning. The code also predicts whether the pressure tube will rupture prior to contacting the calandria tube or balloons into contact with the calandria tube.

SMARTT is a two dimensional code which models one-half of the fuel bundle with symmetry assumed across the vertical diameter. The code can model either 37-element or 28-element fuel bundles. The model includes a circumferentially and radially conducting pressure tube with 16 full fuel-element and 5 half-element models for the 37-element bundle and 14 full fuel-element models for the 28-element bundle. Figure 1 shows the azimuthal nodalization of a 28-element fuel bundle. The code has been modified to simulate the experimental geometry and the material used in the fuel-element simulators (heaters).

Each fuel element simulator is divided into eight, equal, azimuthal nodes which are subdivided into six radial nodes: four for the graphite heater and one each for the alumina insulator and the Zircaloy sheath. The pressure tube is divided into thirty-two equal azimuthal nodes each of which is subdivided into four radial nodes. The flow cross-sectional area is divided into forty-two subchannels.

Radial and azimuthal conduction is taken into account within each fuel element and the pressure tube. Radiation between the outer surface nodes of all fuel elements and the inner surface nodes of the pressure tube is also accounted for through a radiation-view-factor matrix with the assumption of diffuse, isothermal, grey surfaces. Convective heat transfer between the steam coolant and both the fuel element sheaths and the pressure tube is calculated assuming laminar flow. Heat generation due to the Zircaloy-steam reaction on the sheath outer surfaces and the pressure tube inner surface is modelled with the Urbanic-Heidrick correlation [10]. Heat transfer by radiation and conduction across the gas gap between the pressure tube and the calandria tube is also accounted for.

SMARTT employs a finite difference technique to solve the heat conduction equations within the fuel elements and the pressure tube. A sparse matrix solver is used to simultaneously determine the temperatures of all nodes within each fuel element and the pressure tube at each time step. An iteration scheme permits the use of temperature-dependent material properties which are evaluated at the current temperature. The temperature of each subchannel is calculated as the weighted average of the temperatures of the surface nodes of each fuel element that borders the subchannel.

The calculation of the transverse pressure tube strain is based on the creep constitutive equations of Shewfelt et al. [11]. These creep constitutive equations have been verified against experiments [12]. The pressure tube strain is evaluated in the SMARTT code by employing the code NUBALL [13] as a subroutine with the same pressure tube nodalization as SMARTT. This approach provides both the average pressure tube strain as a function of time, and the local strain (wall thinning) at each circumferential node. Based on these information, it is possible to determine whether or not the pressure tube achieves sufficient average strain to remain circular and contact the calandria tube (about 16.4% average strain), before local wall thinning at the hot spot causes the pressure tube to rupture (local strain at any node reaches 100% true strain before contact with the calandria tube).

DESCRIPTION OF EXPERIMENTAL APPARATUS AND INSTRUMENTATION

The apparatus for this experiment represented a section of a Pickering-type CANDU fuel channel. It consisted of a 2105 mm long section of Zr-2.5 Nb pressure tube containing the 28 fuel element simulators (FES) surrounded by a 1780 mm long Zircaloy-2 calandria tube. The pressure tube used in this experiment was hydrided in a furnace to a nominal value of 200 μg/g dissolved hydrogen. The pressure tube was mounted eccentrically inside the calandria tube simulating a sagged pressure tube geometry where a garter spring is in direct contact with the calandria tube. The gaps between the pressure tube and the calandria tube at the top and the bottom were 12.2 mm and 5 mm, respectively. The calandria tube was surrounded by heated, stagnant water in an open tank which simulated the moderator. The top surface of the calandria tube was covered by at least 65 mm of water during the experiment. The annulus between the pressure tube and calandria tube contained an Inconel X-750 garter spring located at the centre of the test section.

The test section, shown in Figure 2, was closed at one end and connected to a vertical exit pipe at the other end. The exit pipe was connected to a condenser and a surge tank to control the test section pressure. The steam mass flow rate was derived from differential pressure measurements at an orifice plate in the outlet piping.

Five spacer plates, made of 0.9 mm thick Zircaloy-4 plate, were positioned at 450 mm intervals in the heated zone of the test section. Their purpose was to simulate the effects of CANDU bundle end plates, radially position the FES bundle and to help minimize FES sag at high temperatures. Holes were drilled in the spacer plates to allow for steam flow between the FES rings. The flow distribution through the various FES flow rings was designed to approximate, as closely as possible, the flow away from the end plate in an actual 28-element fuel bundle.

The FESs were arranged as a typical 28-element Pickering type CANDU fuel bundle. Each FES consisted of Zircaloy-4 cladding (15.2 mm OD, 14.4 mm ID) within which annular Alumina pellets (14.3 mm OD, 6.1 mm ID, and 16 mm long) electrically insulated the cladding from a graphite rod heater. The graphite heaters, 6 mm in diameter, 1800 mm in length, were coated with tungsten carbide to minimize the high temperature reaction between the graphite and alumina.

The FESs were connected in parallel to a DC power supply. The voltage drop across each FES ring was measured through voltage taps placed on the power supply connections. Current through the FESs was derived from voltages measured across load carrying shunts for each ring of heaters. Resistance and power were calculated from the measured voltage and current. Power distribution throughout the FES bundle was designed to be similar to that found in a Pickering-type fuel bundle. Design targets for normalized element powers were 1.111, 0.894, and 0.775 for the outer, middle and inner FES rings, respectively.

The heated length of the test section was instrumented at five distinct axial locations (Ring 1 to Ring 5 in Figure 2). The detailed radial locations of thermocouples at each axial location (Ring 1 to Ring 5) are shown in Figure 3. Thermocouples were used to measure the temperatures of the FES cladding (12 thermocouples), pressure tube (32 thermocouples), calandria tube (3 thermocouples), exit steam (2 thermocouples) and water in the tank surrounding the calandria tube (3 RTDs). The thermocouples on the FESs and the pressure tube were 0.5 mm OD Inconel-clad, K-type (chromel-alumel) with magnesium oxide insulation. The thermocouples used on the calandria tube were made from fibreglass insulated K-type with wire diameters of 0.13 mm. The temperatures of the exit steam and the water surrounding the calandria tube were measured with K-type sheathed thermocouples.

Three Linear Variable Differential Transformers (LVDTs) were installed to monitor pressure tube movement relative to the calandria tube. LVDTs 1 and 2 were located near axial location Ring 2, 455 mm from the closed end, and measured the top and bottom movement of the pressure tube, respectively. The third LVDT was located on the top of the pressure tube near axial location Ring 4, 1130 mm from the closed end.

EXPERIMENTAL PROCEDURE

The following procedures were used for this test :

1 - The annulus between the pressure and calandria tubes was purged with CO_2.
2 - The purge flow was high initially but reduced to near stagnation before the start of the test.
3 - The water surrounding the calandria tube was stirred and heated to 80°C for degassing and allowed to cool down to 75°C before the start of the test.
4 - The test section and exit piping were filled with water and pressurized to 4.0 MPa for this experiment.
5 - The temperature of the pressurized water was gradually raised to the saturation temperature using a 5 kW electric heater.
6 - The test was started by opening the steam outlet valve and increasing the test section power by applying a pre-specified transient power history. Test section power and pressure were manually controlled to maintain steady state values.
7 - The test was terminated by reducing the power after the pressure tube had fully ballooned into contact with

the calandria tube.

EXPERIMENTAL RESULTS

The channel pressure in this experiment was constant at 4.0 MPa. The transient power history is shown in Figure 4. The maximum power input to the heaters was 200 kW. When the power ramp began around 10 s into the experiment, the water started to boil off and the outlet steam flow rate peaked at about 63 g/s at about 70 seconds when the power setting was constant at 200 kW. As the upper part of the pressure tube and fuel elements became uncovered, the temperature at the top increased while the bottom of the pressure tube remained at the coolant saturation temperature. As the water in the channel continued to boil off, a significant circumferential temperature gradient developed around the pressure tube.

The average heat up rate at the top of the channel was 4°C/s. The temperature profiles show similar circumferential temperature gradients occurred at the various axial locations with only a slight time delay (about 5 s) in ballooning time at the steam exit end. The pressure tube ballooned into contact with the calandria tube at 219 s at axial location Ring 1 and at 224 s at Ring 5. The maximum recorded contact temperatures were 748°C and 745°C, for axial locations Ring 1 and Ring 5, respectively. The maximum top-to-bottom circumferential temperature gradients on the pressure tube at Ring 1, 20° from the top, and Ring 5, at the top, prior to ballooning contact, were 439°C and 396°C, respectively. The pressure tube temperatures at the top decreased sharply following the contact with the calandria tube. As a result of the contact with the calandria tube, the thermocouples on the outer surface of the pressure tube were shorted out and their subsequent measurements were invalidated.

The temperature increases on the sheaths indicate when the FESs became dry. The corresponding thermocouple locations were then used to infer water level in the pressure tube during the experiment. The maximum sheath temperature recorded at Ring 1 was 1050°C at the time of pressure tube/calandria tube (PT/CT) contact. Before the end of the test sheath temperatures had reached approximately 1230°C at this location .

The calandria tube temperature increased to 488°C and 511°C at axial locations Ring 1 and Ring 5, respectively, after PT/CT contact indicating localized film boiling and subsequent rewetting of this area. This was confirmed by the post test observation of a slight local discolouration of the calandria tube surface. Similar areas of discolouration were noted along the pressure tube, near the top, particularly in the region close to the steam exit line.

SMARTT CODE MODIFICATIONS AND ASSUMPTIONS

Two modifications were made to the code for the simulation of the present experiment. The internal geometry and material of the fuel-element simulators replaced those of the CANDU fuel. Originally, the code was capable of modelling seven discrete liquid levels from 100% to 0% liquid in the channel. To increase the accuracy of the liquid level representation, the code was modified to allow for fifteen (seventeen for a 37-element bundle) discrete liquid levels which improved the accuracy of the code predictions for relatively slowly decreasing liquid levels.

The discrete liquid levels in SMARTT are set by the nodalization of the channel flow area into subchannels. The liquid levels modelled are: 100%, 97%, 95%, 92%, 86%, 78%, 69%, 60%, 50%, 41%, 31%, 22%, 14%, 8%, 5%, 3% and 0% for the 37-element model. For the 28-element model, the liquid levels are: 100%, 97.3%, 93.5%, 90.7%, 82.2%, 70.5%, 61.1%, 50.0%, 38.9%, 29.5%, 17.8%, 9.3%, 6.5%, 2.7% and 0.0%. The percentages indicate the fraction of total channel cross-sectional flow area covered by the liquid. The falling liquid level is simulated by switching instantaneously from one level to the next.

The following assumptions are used in the simulation of this experiment:

1 - The steam averaging procedure was used in the steam-filled subchannels to determine the coolant temperature.
2 - The emissivity of the fuel element simulators was assumed to be 0.6 and the emissivity of the pressure tube

was assumed to be 0.8. The emissivity of the calandria tube was taken to be 0.33.

3 - The calandria tube temperature was held constant at the temperature of the liquid in the water tank for this experiment.

4 - The Urbanic-Heidrick correlation [10] was used to calculate the Zircaloy-steam reaction rate.

5 - The flow was assumed to be laminar in the steam-filled subchannels and a Nusselt number of 4.0 was used to calculate the sheath-to-coolant heat transfer coefficients. The coolant-to-pressure tube heat transfer coefficients were set equal to the sheath-to-coolant heat transfer coefficients in the outer subchannels.

6 - The channel pressure and the power history measured in the experiment were input directly into the SMARTT code.

7 - The failure criterion used for the pressure tube rupture was 100% local true strain (i.e. failure is assumed when the local thickness is reduced to 37% of its nominal value).

8 - The ballooning criterion used for the pressure tube contact with the calandria tube was 16.4% average diametral strain.

9 - The inferred liquid level determined from both sheath and pressure tube thermocouple measurements was used in these simulations and was directly input to the SMARTT code. The water level was assumed to be 100% at the start of the experiment.

10 - The SMARTT code liquid levels were dropped from one discrete level to the next when the inferred liquid level became approximately halfway between the two discrete levels.

COMPARISON WITH EXPERIMENTAL RESULTS

Power, pressure and channel liquid level transient are required as input to the SMARTT code. The power transient and pressure were obtained directly from the measured values. The radial power distributions measured in the experiment were used as input to the SMARTT code.

The pressure in this experiment was kept constant. The liquid level was inferred from the plots of the height of various thermocouples above the bottom of the pressure tube versus the time at which the thermocouple started to indicate increasing temperatures above that of the coolant saturation temperature. This time was interpreted as the time at which the level dropped below that particular thermocouple position (Figure 5).

Two parameters are chosen to show the comparison between the SMARTT predictions and the experimental results, namely, the pressure tube and the heater sheath temperature transients. The SMARTT simulation always ends when the pressure tube fails or balloons into contact with the calandria tube.

SMARTT predictions are compared against the pressure tube temperature measurements at three axial locations (Rings 1, 3 and 5) and at six circumferential positions (0°, 60°, 80°, 100°, 120° and 180°) as shown in Figures 6 to 8. The experimental results show that the top of the pressure tube, Ring 1 (Figure 6), reached about 731°C at 219 s at which time the thermocouple failed. The temperatures at the other circumferential locations start to peak at later times in succession and then start to fall after the pressure tube ballooned into contact with the calandria tube. This is an indication that the contact occurred first at the top and then spread circumferentially toward the bottom of the pressure tube. This trend is best seen in Figure 8 where thermocouple failure occurred at a later time at the 80° circumferential location. The contact then spread axially and circumferentially over the next few seconds until the pressure tube had fully ballooned into contact with the calandria tube.

The SMARTT prediction of the pressure tube temperature lags the experimental measurements in the upper half of the tube in the early part of the transient. In the later stages of the heatup, the pressure tube temperature becomes overpredicted at the top at all axial locations when the liquid-level in both SMARTT and the experiment reaches zero. The SMARTT simulation predicted that the pressure tube reached a maximum temperature of 781°C at the top and it ballooned into contact with the calandria tube as the average diametral strain reached 16.4%. The simulation predicted that the contact time was 214 s as compared with 219 s and 224 s at axial locations Ring 2 and Ring 4, respectively, in the experiment. However, the maximum local pressure tube strain was predicted to be 85% at the top of the tube. The nonuniform circumferential ballooning observed in the experiment is not modelled in

SMARTT as the code assumed the pressure tube remained circular and concentric during ballooning. This assumption resulted in circumferential pressure tube/calandria tube (PT/CT) contact once the ballooning criterion is satisfied. For that reason the code prediction indicates that the ballooning occurs at the same time at all circumferential locations (Figures 6 to 8).

Figures 9, 10, and 11 show the comparison between experimental measurements and SMARTT predictions of the pressure tube circumferential temperature profiles at axial Rings 1, 3, and 5, respectively. The maximum top-to-bottom pressure tube circumferential differential temperatures measured and predicted were 439°C and 412°C, respectively. The code predictions were in good qualitative agreement with measurements at all axial locations; however, the magnitude of the gradient was overpredicted. The measured maximum top-to-bottom pressure tube differential temperature appears to have been nearly constant along the length of the channel.

Figures 12 and 13 show the comparison between experimental measurements and SMARTT predictions for the sheath temperatures at axial Rings 1 and 3. These were the only reliable measurements reported in the experiment since various thermocouples failed at different stages of the experiment. At the time of pressure-tube/calandria-tube contact, the maximum measured sheath temperature was 1050°C at Ring 1, TC10. The maximum sheath temperature was predicted by SMARTT at pin #1, node #4 (see Figure 1) on the inner surface of the outer fuel-element ring. The predictions at the end of the simulation (214 s) are in excellent agreement with the measured sheath temperatures at both Rings 1 and 3. Early in the transient the simulation lags the measured sheath temperatures in the upper half of the bundle because the liquid-level transient in the simulation was heavily weighted towards the pressure tube rather than sheath thermocouples.

In general, good overall agreement between experimental measurements and SMARTT predictions was achieved in this analysis. The detailed comparison made between measurements and predictions for the pressure tube and sheath temperatures and the time of ballooning shows that the models and assumptions used in this analysis were appropriate and provided a reasonable representation of the experimental conditions, even though the eccentricity of the pressure tube was not modelled in this analysis due to code limitations.

COMPARISON BETWEEN HYDRIDED AND AS-RECEIVED PRESSURE TUBE

The first supplementary boil-off experiment S-5-1 which used an as-received pressure tube was analyzed using the SMARTT code and the results were compared with experimental measurements [1]. Figure 14 shows a comparison between SMARTT predictions and the pressure tube temperature measurements at axial location Ring 5 for five circumferential positions (0°, 60°, 100°, 120° and 180°). Figure 15 shows a comparison between experimental measurements and SMARTT predictions for the sheath temperatures at axial location Ring 3.

Comparison of Figure 8 for the hydrided pressure tube and Figure 14 for the as-received pressure tube shows that the heat up is similar; peak pressure tube temperatures are within 20°C; and top-to-bottom thermal gradients are within 30°C. In both experiments, the pressure tube did not rupture and ballooned into contact with the calandria tube in approximately the same time interval after the channel started to void. The comparison of the heatup and peak sheath temperatures in Figures 13 and 15 also shows a very similar trend. At the time of PT/CT contact, the peak sheath temperatures are 1040°C and 1130°C in Figure 13 and Figure 15, respectively. Figure 16 shows the displacement of the top of the pressure tube during ballooning and the SMARTT predictions for both experiments. The results for the as-received pressure tube have been shifted in time to make the experimentally observed times of PT/CT contact coincide. Table 1 summarizes the comparison between the two experiments.

The conclusion of this comparison is that the addition of 200 μg/g dissolved hydrogen in the pressure tube produces no significant effect on the creep behaviour of the pressure tube during the ballooning process under large LOCA conditions. The thermal behaviour of the pressure tube also showed no significant indication that it was affected by the dissolved hydrogen content in the pressure tube. Thus, pressure tubes which have absorbed up to 200 μg/g dissolved hydrogen would be expected in a postulated LOCA scenario to exhibit behaviour similar to an "as-received" pressure tube.

A number of areas for future development in the SMARTT code have been identified as a result of this analysis. These include the lack of feedback between geometry changes and the effect on thermohydraulic conditions and thermal radiation calculations, the lack of capability to model an eccentric pressure/calandria tube geometry, the assumption of circular deformation made in the pressure tube deformation model, and the inability to model the effect of axial variation in thermohydraulic conditions. The implementation of these modifications will enhance the code's ability to accurately model progressive contact between the pressure and calandria tubes and the coupling between thermohydraulic conditions and geometry changes.

CONCLUSIONS

1 - The SMARTT code was used to model the latest 28-element boil-off experiment with hydrided pressure tube which is an extension of the pressure tube circumferential differential temperature experimental program. The code was modified to model the improved heater geometry used in the experiment and to increase the number of discrete liquid levels from 7 to 15 for more accurate representation of the actual liquid level in the experiment.

2 - In general, good agreement was obtained between experimental results and SMARTT predictions. The discrepancies are attributed to the difficulty in accurately determining the liquid level transient and to the method of instantaneously dropping the liquid level which is used in the code instead of the actual continuous, smooth decrease in liquid level experienced by the fuel-element simulators and the pressure tube in the experiment.

3 - The pressure tube ballooned into contact with the calandria tube. The ballooning process started at the top and then spread both circumferentially and axially.

4 - The effect of dissolved hydrogen in the pressure tube was examined with a comparison between the hydrided pressure tube and an as-received pressure tube under identical experimental conditions. Similar behaviour was observed for both tubes in the two experiments. The experimental and simulation results indicate no significant effect on the pressure tube thermal and mechanical behaviour due to the dissolved hydrogen concentration.

5 - Modelling is underway to implement the feedback effect between geometry changes and thermohydraulic response in the channel. The other improvements which were identified will be implemented in the near future.

REFERENCES

[1] BAYOUMI M.H. et al., "Simulation of the Pressure Tube Circumferential Temperature Distribution Experiments (Boil-Off Experiments)", 4th International CNS/ANS Conference on Simulation Methods in Nuclear Engineering, Montreal, June 1993.

[2] LOCKE K.E. et al., "SMARTT - A Computer Code to Predict Fuel and Pressure Tube Temperature Gradient Under Asymmetric Coolant Conditions", Proc. 6th Annual CNS Conference, Ottawa, June 1985.

[3] HUSSEIN E. and LUXAT C.J., "Fuel Cooling Under Steam Venting Conditions", Proc. 6th Annual CNS Conference, Ottawa, June 1985.

[4] ARCHINOFF G.H. et al., "Simulation Methodology for Pressure Tube Integrity Analysis and Comparison With Experiments", Proc. 2nd International CNS/ANS Conference on Simulation Methods in Nuclear Engineering, Montreal, October 1986.

[5] LOCKE K.E. et al., "Progress on SMARTT Simulation of Pressure Tube Circumferential Temperature Distribution Experiments - Test 1 to 4", Proc. 8th Annual CNS Conference, New Brunswick, June 1987.

[6] YUEN P.S. et al., "The Experimental Measurement of Circumferential Temperature Distributions Developed on Pressure Tubes Under Stratified Two-Phase Flow Conditions", Proceeding of the 10th Annual CNS

Conference, Ottawa, June 1989.

[7] BAYOUMI M.H. et al., "Further Simulation of the Pressure Tube Circumferential Temperature Distribution Experiments (Make-Up Water Series)", Proc. 13th Annual CNS Conference, New Brunswick, June 1992.

[8] BAYOUMI M.H. et al., "Simulation of the Pressure Tube Circumferential Temperature Distribution Experiments (Variable Make-Up water Experiments)", INC93, International Nuclear Congress and Exhibition, Toronto, Ontario, Canada, October 1993.

[9] BAYOUMI M.H. et al., "Simulation and Investigation of the Pressure Tube Circumferential Temperature Distribution Experiments (Boil-Off Experimental Series)", 14th CNS Conference, Montreal, June 1994.

[10] URBANIC V.F. and HEIDRICK T.R., "High-Temperature Oxidation of Zircaloy-2 and Zircaloy-4 in Steam", Journal of Nuclear Materials, V. 75, pp. 251-261.

[11] SHEWFELT R.S.W. et al., "A High Temperature Creep Model for Zr-2.5 wt% Nb Pressure Tubes", Journal of Nuclear Material, V. 125, 1984, pp. 228-235.

[12] SHEWFELT R.S.W. and GODIN D.P., "Verification Tests for GRAD, A Computer Program to Predict the Non-uniform Deformation and Failure of Zr-2.5 wt% Nb Pressure Tubes During a Postulated Loss-of-Coolant Accident", AECL-8384.

[13] KUNDURPI P.S., "Validation of the Computer Code for Simulation of Pressure Tube Asymmetric Ballooning Behaviour", Proc. 12th Annual Symposium on Simulation of Reactor Dynamics and Plant Control, Hamilton, April 1986.

TABLE 1
Comparison of "As-received" and "Hydrided" Pressure Tube Experiments

Parameter	Hydrided PT	As-received PT
PT heating rate (°C/s)	4.0	4.2
Max. PT temperature (°C)/Location	748/Ring 1	771/Ring 5
Max. sheath temperature at time of PT/CT contact (°C)/Location	1070/Ring 1	1130/Ring 3
Max. PT strain (%)	54	54
Ballooning Time (s)	218 - 224	214 - 224
Power (kW/m)	111	106
Max. top-to-bottom temperature gradient before contact (°C)	439	410

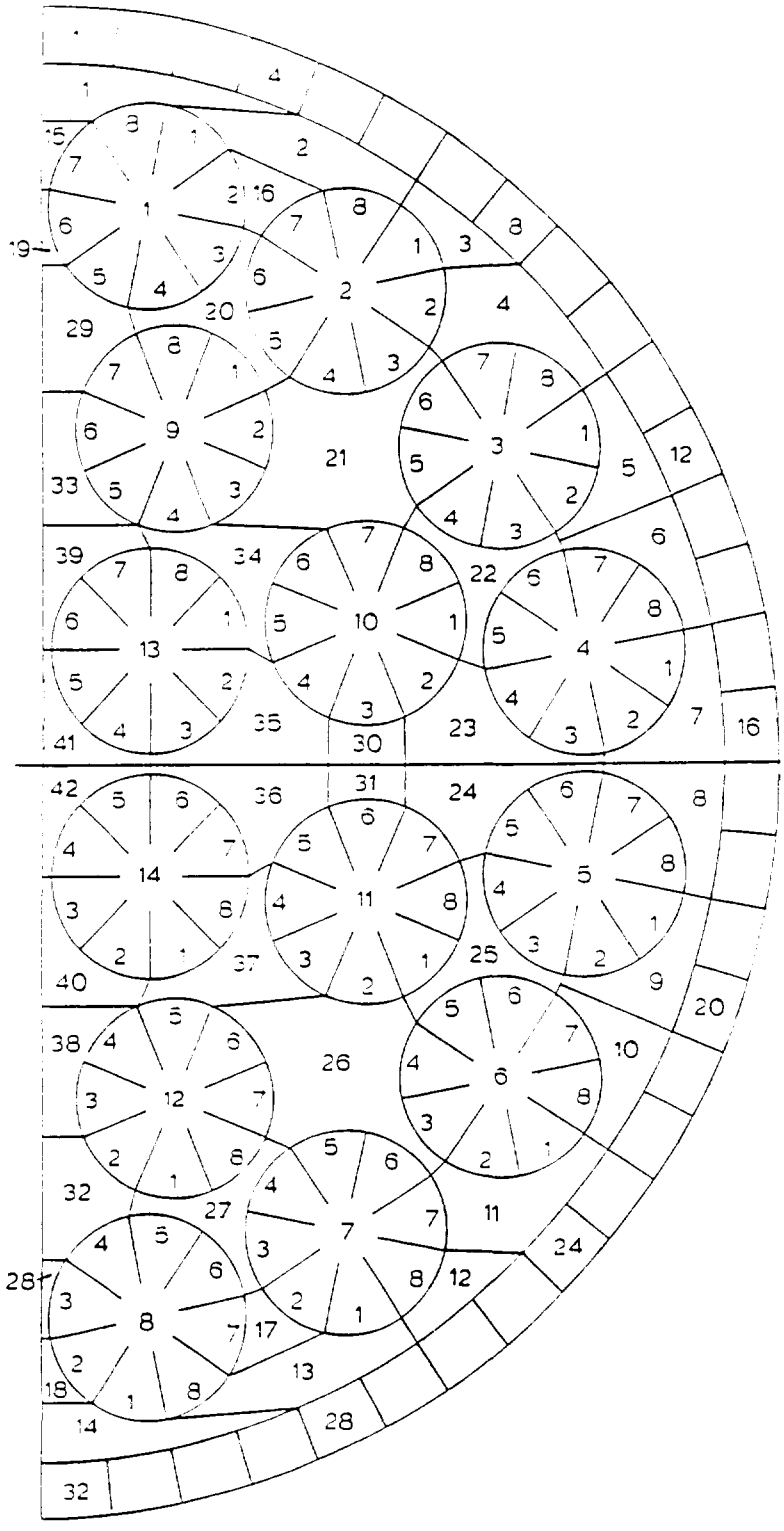

Figure 1: Diagram of 28-element half-bundle model showing fuel element, pressure tube, and subchannel nodalization for SMARTT.

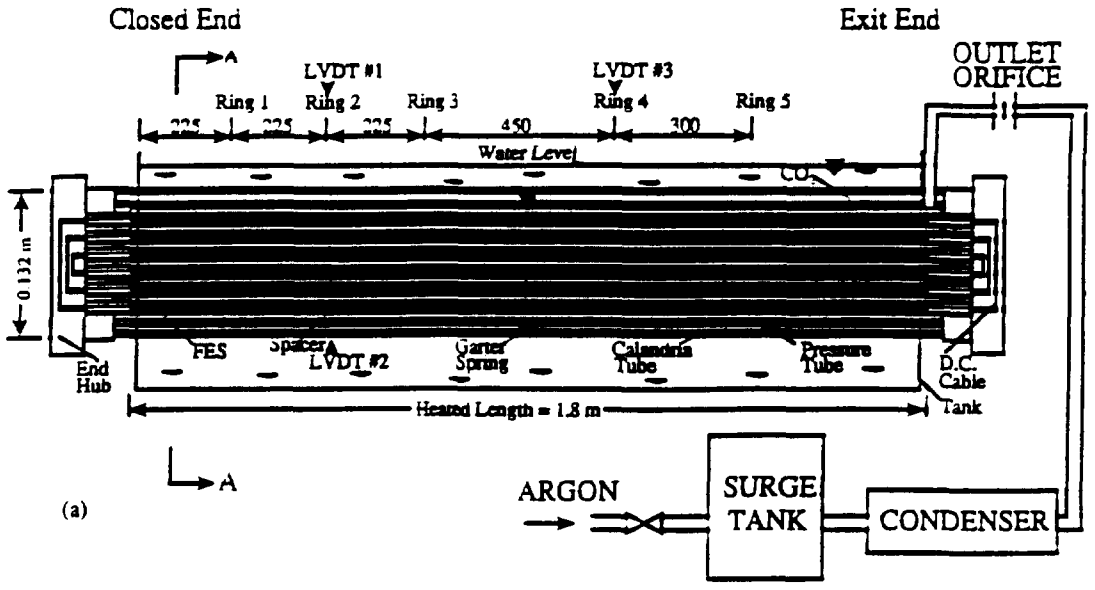

Figure 2: Schematic diagram of test section showing location of instrumented axial locations (Rings 1 to 5).

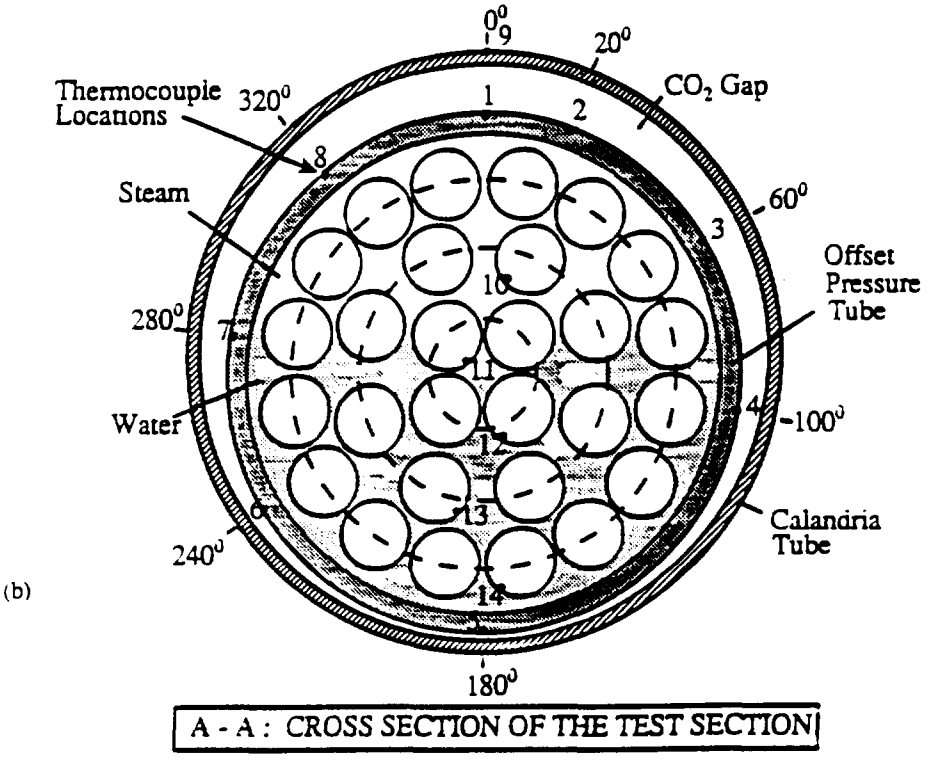

Figure 3: Cross-sectional view of test section showing location of thermocouples at each instrumented axial location.

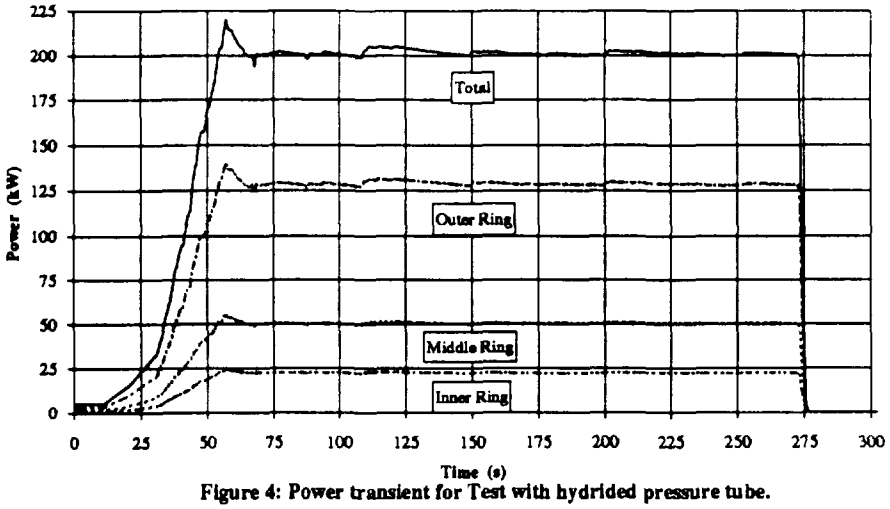

Figure 4: Power transient for Test with hydrided pressure tube.

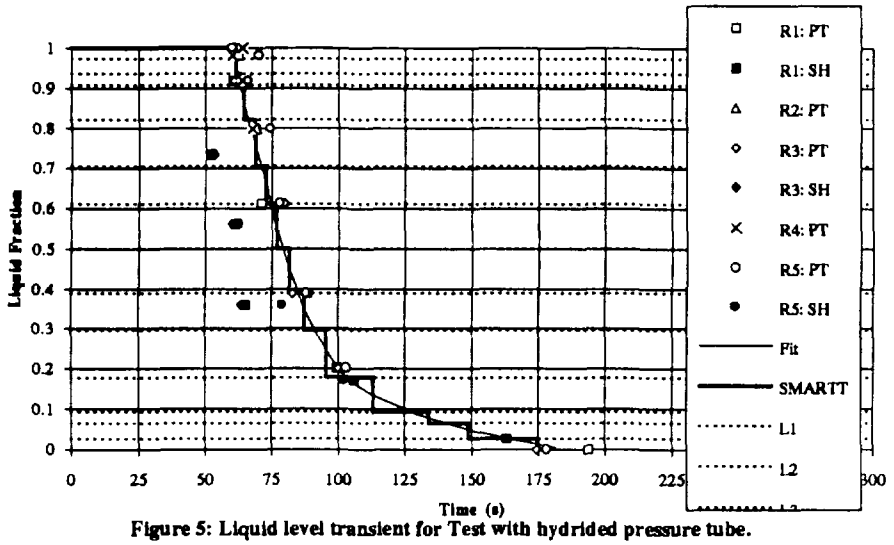

Figure 5: Liquid level transient for Test with hydrided pressure tube.

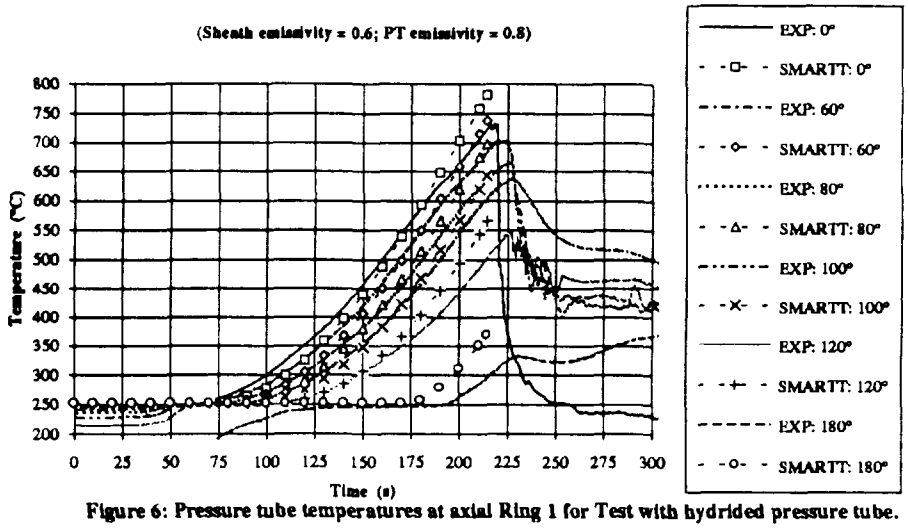

Figure 6: Pressure tube temperatures at axial Ring 1 for Test with hydrided pressure tube.

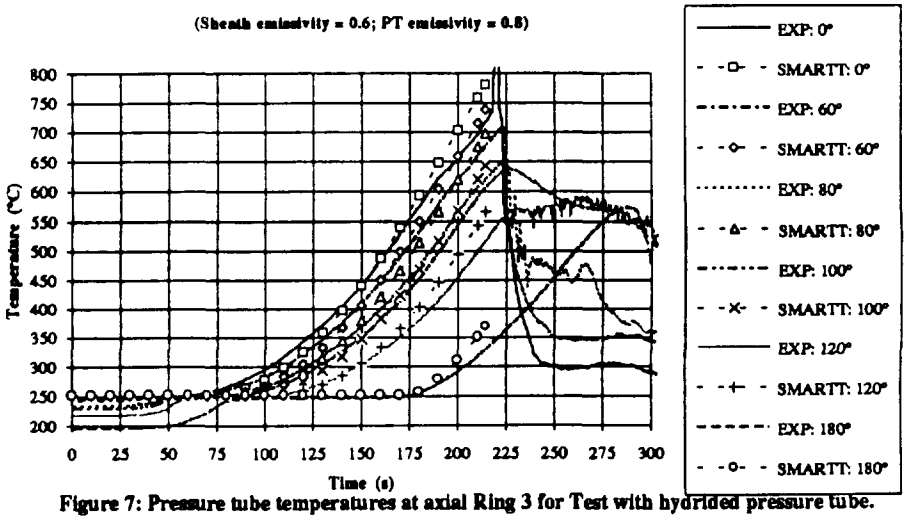

Figure 7: Pressure tube temperatures at axial Ring 3 for Test with hydrided pressure tube.

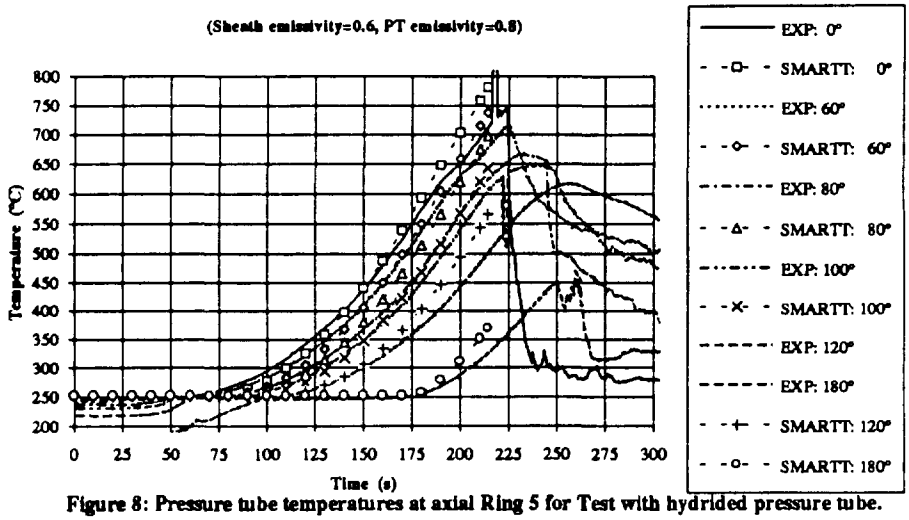

Figure 8: Pressure tube temperatures at axial Ring 5 for Test with hydrided pressure tube.

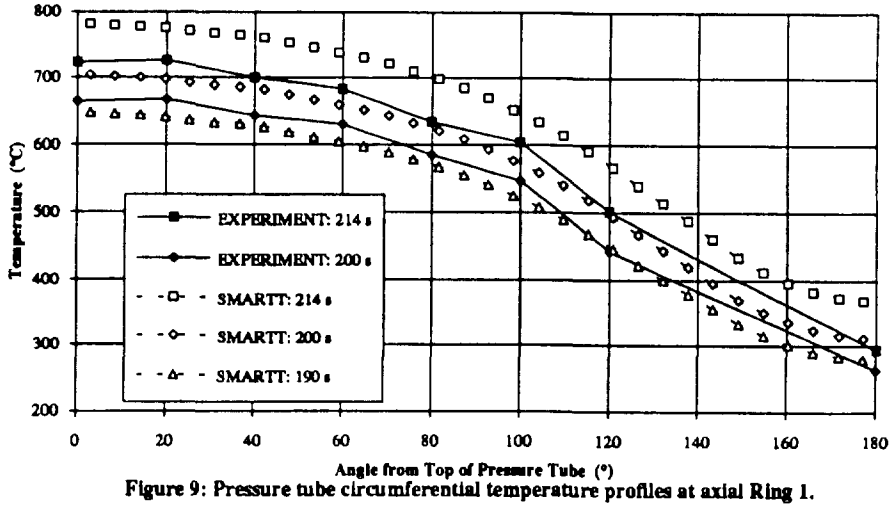

Figure 9: Pressure tube circumferential temperature profiles at axial Ring 1.

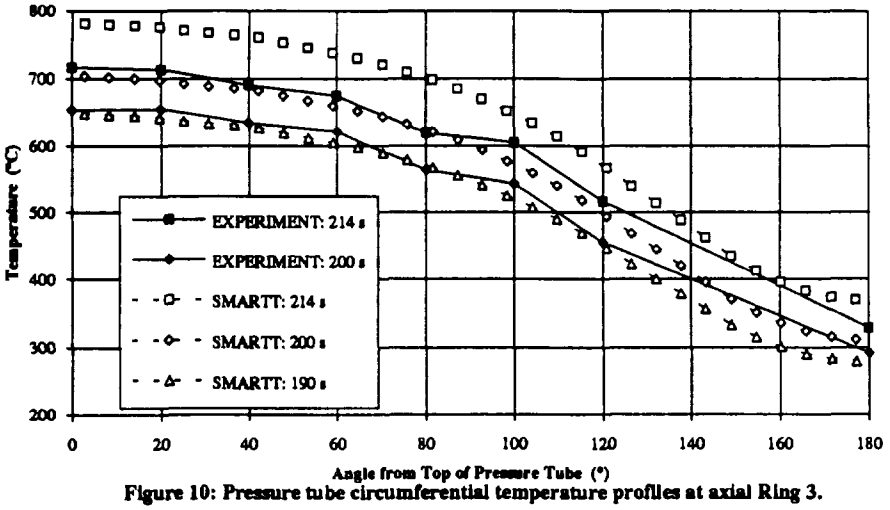

Figure 10: Pressure tube circumferential temperature profiles at axial Ring 3.

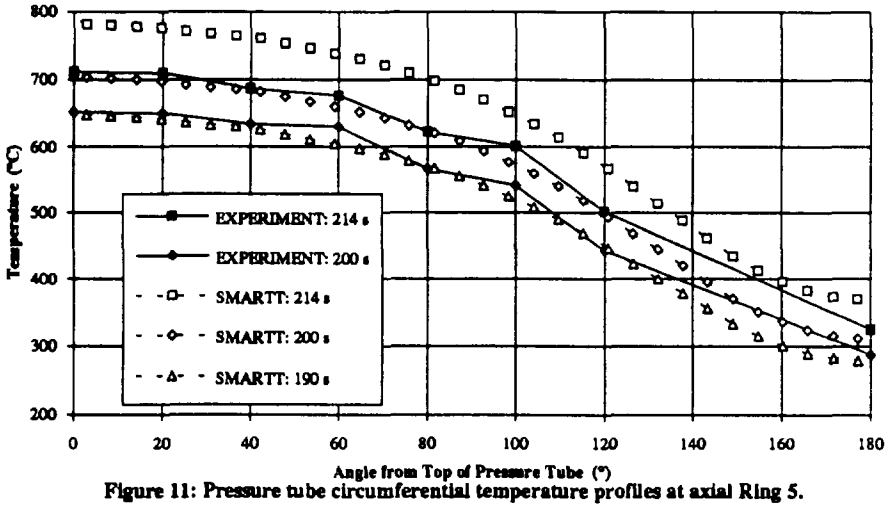

Figure 11: Pressure tube circumferential temperature profiles at axial Ring 5.

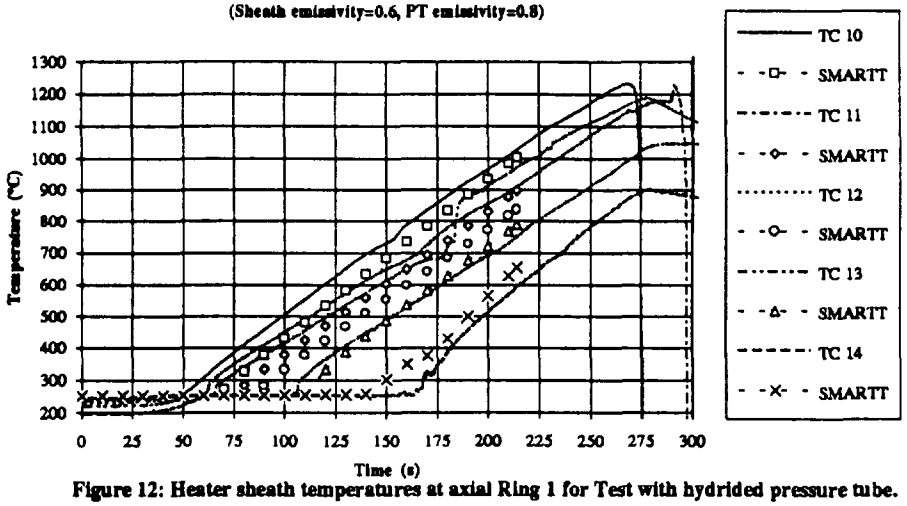

Figure 12: Heater sheath temperatures at axial Ring 1 for Test with hydrided pressure tube.

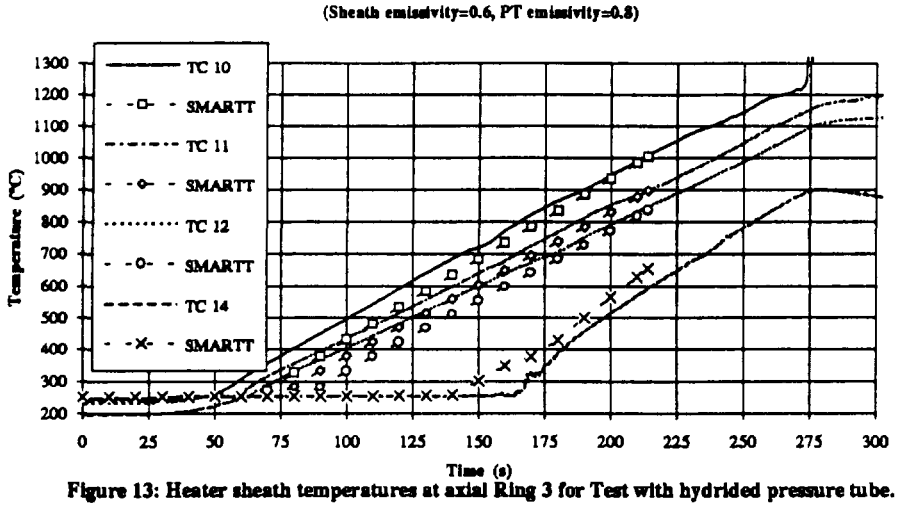

Figure 13: Heater sheath temperatures at axial Ring 3 for Test with hydrided pressure tube.

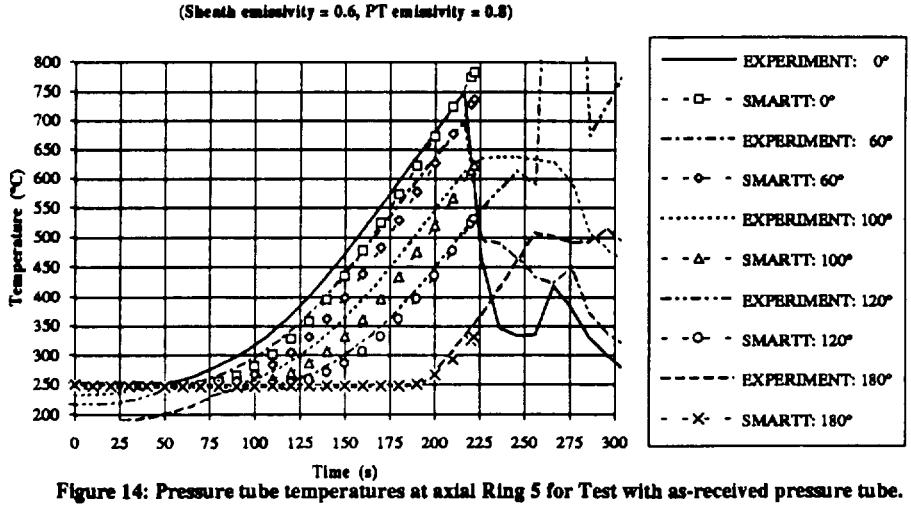

Figure 14: Pressure tube temperatures at axial Ring 5 for Test with as-received pressure tube.

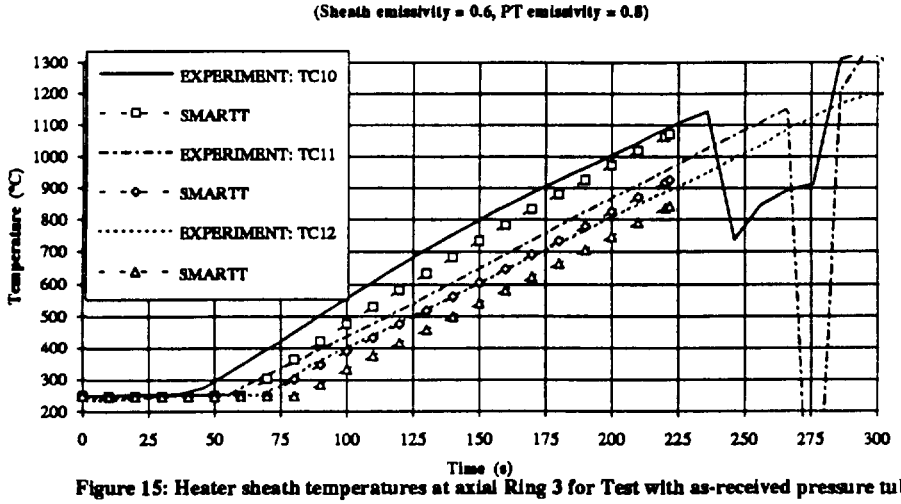

Figure 15: Heater sheath temperatures at axial Ring 3 for Test with as-received pressure tube.

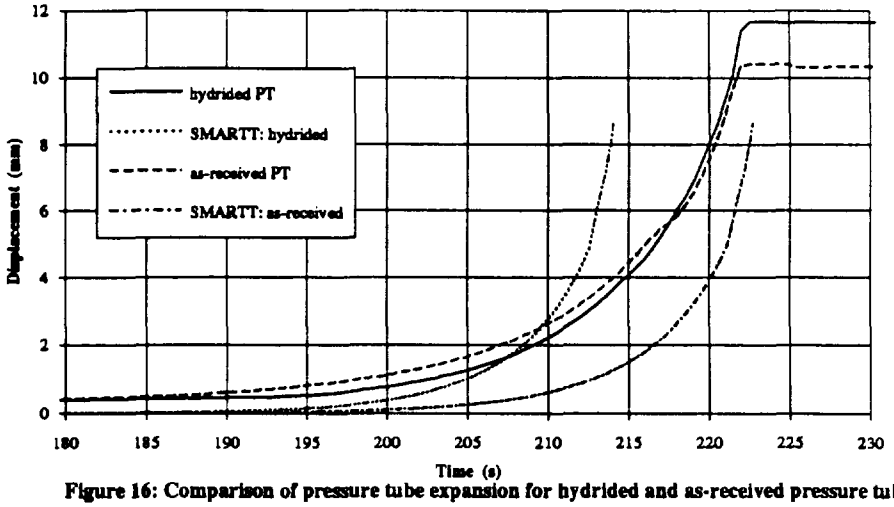

Figure 16: Comparison of pressure tube expansion for hydrided and as-received pressure tubes.